Cancer Science
The official journal of the Japanese Cancer Association

Non-thermal DNA damage of cancer cells using near-infrared irradiation

Yohei Tanaka,[1,4] Naoto Tatewaki,[2] Hiroshi Nishida,[2] Takahiro Eitsuka,[2] Nobuo Ikekawa[2] and Jun Nakayama[3]

[1]Clinica Tanaka Plastic, Reconstructive Surgery and Anti-aging Center, Matsumoto, Nagano; [2]Department of Applied Life Sciences, Niigata University of Pharmacy and Applied Life Sciences, Niigata; [3]Department of Molecular Pathology, Shinshu University Graduate School of Medicine, Matsumoto, Nagano, Japan

(Received November 18, 2011/Revised April 2, 2012/Accepted April 14, 2012/Accepted manuscript online April 19, 2012/Article first published online May 17, 2012)

Previously, we reported that near-infrared irradiation that simulates solar near-infrared irradiation with pre- and parallel-irradiational cooling can non-thermally induce cytocidal effects in cancer cells. To explore these effects, we assessed cell viability, DNA damage response pathways, and the percentage of mitotic cancer cells after near-infrared treatment. Further, we evaluated the anti-cancer effects of near-infrared irradiation compared with doxorubicin in xenografts in nude mice by measuring tumor volume and assessing protein phosphorylation by immunoblot analysis. The cell viability of A549 lung adenocarcinoma cells was significantly decreased after three rounds of near-infrared irradiation at 20 J/cm^2. Apoptotic cells were observed in near-infrared treated cells. Moreover, near-infrared treatment increased the phosphorylation of ataxia-telangiectasia mutated (ATM) at Ser^{1981}, H2AX at Ser^{139}, Chk1 at Ser^{317}, structural maintenance of chromosome (SMC) 1 at Ser^{966}, and p53 at Ser^{15} in A549 cells compared with control. Notably, near-infrared treatment induced the formation of nucleic foci of γH2AX. The percentage of mitotic A549 cells, as measured by histone H3 phosphorylation, decreased significantly after three rounds of near-infrared irradiation at 20 J/cm^2. Both near-infrared and doxorubicin inhibited the tumor growth of MDA-MB435 melanoma cell xenografts in nude mice and increased the phosphorylation of p53 at Ser^{15}, Chk1 at Ser^{317}, SMC1 at Ser^{966}, and H2AX at Ser^{139} compared with control mice. These results indicate that near-infrared irradiation can non-thermally induce cytocidal effects in cancer cells as a result of activation of the DNA damage response pathway. The near-infrared irradiation schedule used here reduces discomfort and side effects. Therefore, this strategy may have potential application in the treatment of cancer. (*Cancer Sci* 2012; 103: 1467–1473)

Near-infrared (NIR) is electromagnetic radiation that simultaneously exhibits both wave and particle properties and is known to be strongly absorbed by water, hemoglobin, and myoglobin. Previously, we reported that NIR irradiation that simulates solar NIR with pre- and parallel-irradiational cooling can penetrate the skin and non-thermally affect the dermis,[1–4] subdermal blood plexus, superficial skeletal muscles,[5,6] and other tissues.[7–10] Furthermore, NIR induces apoptotic changes in both smooth muscle fibers of the subdermal blood plexus and skeletal muscle fibers of the panniculus carnosus in rats, which results in long-lasting vasodilation and muscle thinning.[5,6]

At a wavelength of 904 nm, NIR has been shown to have antitumor activity and to increase cytomorphological changes by inducing apoptosis in neoplastic cells.[11] In addition, actively proliferating cells exhibit increased sensitivity to red and NIR wavelengths.[12,13] It appears that NIR irradiation induces DNA strand breaks and cell death by apoptosis,[14] and can elicit photodisruptive destruction of tumor tissue.[15] However, in-depth studies to date have not explored the optimal NIR wavelength that is most effective for treating cancer.

In a previous study, we found that the NIR spectrum between 1100 and 1800 nm, with water filtering to remove wavelengths between 1400 and 1500 nm, significantly suppresses the proliferation of various cancer cell lines and significantly inhibits the growth of MCF7 breast cancer cells transplanted into SCID mice and MDA-MB435 melanoma cells transplanted into nude mice.[7] We hypothesized that this specialized NIR irradiation may induce DNA damage in cancer cells and therefore provide a potentially effective approach for cancer treatment.

It is well known that DNA damage checkpoint proteins, including ataxia-telangiectasia mutated (ATM), play a pivotal role in the maintenance of chromosomes.[16,17] To avoid the carryover of damaged DNA to the next generation of cells, checkpoint signals provide a safeguard in several critical phases of the cell cycle. The requirement of ATM and downstream molecules for checkpoint activation and cell survival following DNA damage, γ-irradiation, or treatment with genotoxic agents has been well-documented.[18–20] Ataxia-telangiectasia mutated phosphorylates various substrates, including p53, Chk1, and structural maintenance of chromosome (SMC) 1 , and it is therefore important to define that exact biological mechanism taking place in cells treated with NIR irradiation.

To explore the biological effects of NIR irradiation for cancer treatment, we performed both *ex vivo* and *in vivo* testing. The MTT assay was used to investigate the cell viability of cultured cancer cells after they had been treated with NIR irradiation. We also evaluated the percentage of mitotic cancer cells by performing a G_2/M checkpoint analysis and assessed the DNA damage response by immunoblot analysis. Finally, we performed *in vivo* studies to examine the anticancer effects of NIR irradiation compared with doxorubicin by measuring tumor volume and performing immunoblot analysis of samples from xenografts.

Materials and Methods

Near-infrared device. Near-infrared irradiation was performed using a broadband NIR source (Titan; Cutera, Brisbane, CA, USA). The NIR device emits an NIR spectrum between 1100 and 1800 nm, with water filtering to remove wavelengths between 1400 and 1500 nm, and simulates solar NIR radiation that reaches the skin of humans on the Earth's surface. This device delivers NIR without wavelengths that are strongly absorbed by water and hemoglobin, which enables the safe delivery of NIR energy deeper into tissue.

To avoid thermal effects, the sapphire contact cooling tip was set to a fixed temperature of 20°C to provide contact

[4]To whom correspondence should be addressed. E-mail: info@clinicatanaka.jp

doi: 10.1111/j.1349-7006.2012.02310.x

cooling. These specific wavelengths and the cooling system enabled the delivery of NIR to deeper tissues without pain or epidermal burns on the animals.

Near-infrared irradiation and output. In our previous *in vitro* study,[7] we performed 3, 10, and 20 rounds of irradiation using two separate fluence settings per round of 20 and 40 J/cm^2. Three rounds at 20 J/cm^2 appeared to be close to a threshold energy dosage. Significant differences were not observed between 10 and 20 rounds of irradiation. Ten rounds at 20 J/cm^2 achieved a comparable reduction in cell count to that seen following three rounds at 40 J/cm^2. Therefore, in the present *in vitro* study we performed one, two, three, four, five, and 10 rounds of NIR irradiation at 20 J/cm^2.

Previously, we reported that three rounds of NIR irradiation at 20 J/cm^2 were sufficient to induce histological changes in the epidermis of rats,[1] but that higher energies had a greater response and were preferable to see effects in deeper tissues. Therefore, in the present we *in vivo* study we performed NIR irradiation at 40 J/cm^2.

Cell culture. Testing was conducted on cultures of human adenocarcinoma A549 cells (American Type Culture Collection, Manassas, VA, USA). The A549 cells were maintained in DMEM supplemented with 10% FBS and antibiotics (100 μg/mL streptomycin and 100 units/mL penicillin). All cell culture reagents were purchased from Invitrogen (Carlsbad, CA, USA). Cells were seeded in 96-well microtiter plates at a concentration of 5×10^3 cells/well in 100 μL medium. All cells were grown at 37°C in a humidified incubator with 5% CO_2.

Cell proliferation assay. The MTT assay was used to evaluate the effects of NIR irradiation on cell growth. The A549 cells were seeded at a density of 1×10^4 cells/well in a 96-well microtiter plate and cultured for 24 h before being subjected to NIR irradiation (one, two, three, four, and five rounds of 20 J/cm^2. After 72 h incubation, the growth medium was removed and 100 μL of 0.05% MTT solution (Wako Pure Chemical Industries, Tokyo, Japan) was added to the culture. The cells were incubated for an additional 4 h at 37°C and then lysed with 100 μL lysis buffer (20% SDS and 50% *N*,*N*-dimethyl formamide [DMF], pH 4.7). Absorbance was measured at 595 nm using a microplate reader (Bio-Rad Laboratories, Hercules, CA, USA).

***In situ* cell death detection.** The A549 cells were seeded onto poly L-lysine-coated coverslips set in 24-well plate set coverslips (Corning, Tewksbury, MA, USA). After 3 h NIR treatment, cells were fixed for 5 min with cold methanol before being rehydrated with PBS. The coverslips were rinsed with PBS and incubated in permeabilization solution (0.1% Triton X-100, 0.1% sodium citrate) for 2 min on ice. Apoptotic cells were detected by the TUNEL method using the In situ Cell Death Detection Kit (Roche Molecular Biochemicals, Mannheim, Germany). After extensive washing, the nuclei were counterstained with DAPI and the cells were examined and photographed under a fluorescent microscope (Zeiss, Jena, Germany).

Preparation of cell lysates. The A549 cells were treated with or without NIR irradiation (two, six, and 10 rounds of 20 J/cm^2). A specific inhibitor of ATM, KU55933 (10 μM), was added to the culture one hour before NIR irradiation. The cells were then harvested by scraping into ice-cold PBS 1–8 h after NIR treatment. The cell extracts were incubated with immunoprecipitation buffer (10 mM Tris-HCl, pH 7.4, 1 mM EDTA, 1 mM EGTA, 150 mM NaCl, 0.5% Nonidet P-40 [NP-40], 1% Triton X-100, 1 mM phenylmethanesulfonyl fluoride [PMSF], 2 μg/mL pepstatin, 2 μg/mL aprotinin, 10 mM NaF, and 1 mM dithiothreitol [DTT]) for 15 min on ice. The tumor tissue was homogenized in RIPA buffer (50 mM Tris-HCl, pH 8.0, 150 mM NaCl, 0.1% SDS, 0.5% sodium deoxycholate, 1% NP-40, 1 mM PMSF, 2 μg/mL pepstatin, 2 μg/mL aprotinin, 10 mM NaF, and 1 mM DTT) for 20 min on ice. The samples were then centrifuged at 15 500*g*. for 20 min at 4°C and the supernatant was solubilized in 4 × SDS sample buffer (200 mM Tris-HCl, pH 6.8, 8% SDS, 40% glycerol, 3.4 M 2-mercaptoethanol, and bromophenol blue) and stored at −30°C until further use. Protein concentrations were determined using the Bradford protein assay reagent (Bio-Rad Laboratories).

Immunoblot analysis. For immunoblot analysis, 20 μg protein was loaded and separated by SDS-PAGE and then transferred to a 0.45-μm PVDF membrane (Millipore, Billerica, MA, USA) using an electroblotting apparatus (Invitrogen). The membrane was blocked with 5% skim milk in Tris-buffered saline containing 0.1% Tween 20 for 1 h at room temperature. Immunoblotting was performed by incubating the membrane with the following primary antibodies for 16 h at 4°C: anti-phosphorylated (p-) p53 Ser^{15} (Cell Signaling, Danvers, MA, USA), anti-p-SMC1 Ser^{966} (Bethyl Laboratories, anti-p-Chk1 Ser^{317} (Bethyl Laboratories, Montogomery, TX, USA), anti-p-ATM Ser^{1981} (Cell Signaling), anti-γH2AX Ser^{139} (Cell Signaling), anti-tubulin (Cell Signaling), and anti-GAPDH (Cell Signaling). The membranes were then washed with Tris-buffered saline with Tween-20 (TBST) and incubated with horseradish peroxidase-conjugated secondary antibodies (anti-mouse or anti-rabbit IgG; Cell Signaling) for 1 h at room temperature. Target proteins were visualized using an Immobilon Western Chemiluminescent HRP Substrate (Millipore) and X-ray film (Fujifilm, Tokyo, Japan).

Analysis of the G_2/M checkpoint. Detection of phosphorylation levels of histone H3 at Ser^{10} was used to monitor mitosis. After culturing for 48 h, cells were treated with or without NIR irradiation (one, three, five, and 10 rounds of 20 J/cm^2). After 1 h incubation, cells were harvested and fixed with ice-cold 70% ethanol. Membranes were permeabilized with 0.25% Triton X-100 in PBS on ice for 15 min and the cells were then incubated with polyclonal rabbit anti-p-histone H3 (Ser^{10}) antibody (Upstate Biotechnology, Lake Placid, NY, USA) for 4 h and Alexa Fluor 488-conjugated goat anti-rabbit IgG antibody (Invitrogen) for 1 h at room temperature. Cellular DNA was counterstained with 50 μg/mL propidium iodide (PI; Dojindo, Kamimashiki, Japan) for 30 min at room temperature. The stained cells were then analyzed on a flow cytometer (COULTER EPICS XL-MCL; Beckman Coulter, Brea, CA, USA).

Immunocytochemistry. The A549 cells were seeded onto poly L-lysine-coated coverslips set in 24-well plate set coverslips (Corning). After NIR treatment, cells were fixed in cold methanol for 5 min, washed with PBS, and then incubated in PBS containing 0.05% saponin. After treatment with 5% normal goat serum (in PBS) for 15 min, cells were incubated with γH2AX antibody (Cell Signaling) for 4 h at room temperature. Cells were then incubated with Alexa Fluor 488-conjugated secondary antibodies (Zymed Laboratories, South San Francisco, CA, USA) for 1 h at room temperature. After extensive washing, nuclei were counterstained with PI and cells were examined and photographed under a fluorescent microscope (Zeiss).

***In vivo* tumorigenicity and treatment.** Mice were housed in a temperature-controlled environment under a 12-h light–dark cycle, with free access to water and standard mouse chow. Body weight and tumor size were measured every other day. Tumor volumes were calculated using the following formula:

$$4/3 \times \pi \times (\text{longest diameter})/2 \times (\text{shortest diameter})/2 \times (\text{shortest diameter})/2$$

The present study was approved by the Shinshu University Institutional Review Board for Animal Study. National and international principles of laboratory animal care were followed throughout the study. Thirty-five female nude mice (Crlj:CD1-Foxn1nu) were obtained from Charles River

doi: 10.1111/j.1349-7006.2012.02310.x

Laboratories (Yokohama, Japan). MDA-MB435 cells (5.0×10^6 cells/100 μL per mouse) were implanted subcutaneously in the right flank of 7-week-old nude mice. When the tumor volume expanded to approximately 120 mm^3, the 18 mice were divided into three groups ($n = 6$ in each group). This was defined as Day 1 for testing. One group (control group) was left untreated, one group was treated with doxorubicin (DOX; 2 mg/kg, i.p.), and the third group was treated with NIR irradiation. Treatments were performed once daily for 7 days and mice were killed on the 7th day.

Statistical analyses. Statistical analysis was performed using SPSS software (SPSS, Chicago, IL, USA. $P < 0.05$ was considered significant.

Results

Cell viability. The cytotoxicity of NIR treatment of A549 cells was evaluated using the MTT assay. Cell viability decreased significantly after treatment with more than three rounds of NIR treatment at 20 J/cm^2, and was markedly reduced after four and five rounds of treatment. We hypothesized that the decrease in cell viability was related to cellular damage, such as DNA damage, induced by NIR irradiation in the treated cells (Fig. 1a).

Apoptotic cell death. We investigated whether the decrease in cell viability following NIR treatment was due to apoptosis or other types of cell death. The TUNEL method was used to detect *in situ* cell death (Fig. 1b). The results showed that a DNA nick in A549 cells (i.e. TUNEL-positive cells) was detected after two and six rounds of NIR treatment, becoming obvious after six rounds of NIR. This indicates that NIR treatment induces apoptotic cell death in a dose-dependent manner, which results in decreased cell viability.

Immunoblot analysis of NIR irradiation-treated A549 cells. To clarify whether NIR can induce a DNA damage response in cells, including the checkpoint signaling pathway, phosphorylation of H2AX at Ser^{139} was measured as an index of the DNA damage in cells. After NIR treatment, phosphorylation of H2AX occurred after two or more rounds of NIR at 20 J/cm^2. In addition, ATM, a key factor in the DNA damage response, was clearly activated by 2–10 rounds of NIR treatment, as shown by the increase in Ser^{1981} phosphorylation (Fig. 2a). The ATM-specific inhibitor KU55933 markedly decreased the phosphorylation of ATM after NIR treatment. In addition, the increases in ATM phosphorylation and the inhibition of phosphorylation by the ATM inhibitor were confirmed in other checkpoint proteins after NIR irradiation (two, six, and 10 rounds of NIR at 20 J/cm^2), including γH2AX, Ser^{15} of p53, Ser^{966} of SMC1, and Ser^{317} of Chk1, with the effects of NIR irradiation being dose dependent (Fig. 2a). Among, the time dependency of phosphorylation of checkpoint-related molecule was observed by 8 h after NIR treatment but in ATM inhibitor, KU55933 was added to the culture. These results suggest that NIR-induced DNA damage triggered ATM activation and the subsequent downstream activation of other factors in the signaling pathway of the DNA damage response. Therefore, the data indicate that NIR irradiation induces ATM-dependent checkpoint signals by damaging cellular DNA.

Analysis of the G_2/M checkpoint. We further examined the mitotic transition by flow cytometry to assess the effects of NIR on the cellular DNA damage response pathway. The percentage of mitotic A549 cells was evaluated by measuring histone H3 phosphorylation at Ser^{10} and found to be significantly decreased after more than three rounds of NIR irradiation at 20 J/cm^2 ($P < 0.05$; Figs 3,4). These data indicate that the G_2/M checkpoint is activated by NIR-induced DNA damage in order to avoid mitotic error.

Immunocytochemistry. The formation of γH2AX foci in the nucleus is well known as an index of DNA damage after genotoxic treatment. To confirm whether NIR induced DNA damage in A549 cells, we checked the formation of γH2AX foci immunocytochemically (Fig. 4). It was obvious that foci formation occurred after NIR treatment and that it increased with an increase in the number of rounds of treatment. The ATM-specific inhibitor KU55933 (10 μM) decreased the formation of γH2AX foci induced by 10 rounds of NIR. These results clearly show that NIR treatment induced the DNA damage response via activation of the ATM signaling pathway.

Effects of NIR irradiation on tumors transplanted into mice. The mean tumor volume of MDA-MB435 cells transplanted into nude mice in the control group was 121.90 ± 13.48 mm^3 on Day 1 of treatment. The tumor volume increased continuously, reaching 137.88 ± 12.98 mm^3 on Day 5 and 169.27 ± 14.84 mm^3 on Day 7.

The mean tumor volume of MDA-MB435 cells in the DOX-treated groups was 120.77 ± 12.08 mm^3 on Day 1 of treatment. The tumor volume increased steadily, reached a maximum volume of 126.73 ± 14.94 mm^3 by Day 3. The volume then decreased until Day 7 (122.05 ± 20.01 mm^3), when the mice were killed for immunoblot analysis. In contrast, the mean tumor volume in the NIR-irradiated MDA-MB435 group was 121.52 ± 15.58 mm^3 on Day 1 of treatment, peaking at 126.15 ± 14.27 mm^3 by Day 3 of treatment and then decreasing rapidly to a final tumor volume of 104.55 ± 10.70 mm^3 on Day 7, when mice were killed (Fig. 5). Importantly, there were significant difference in tumor volume on Day 7 between the control group and the DOX- and NIR irradiation-treated groups. No side effects were observed during the study.

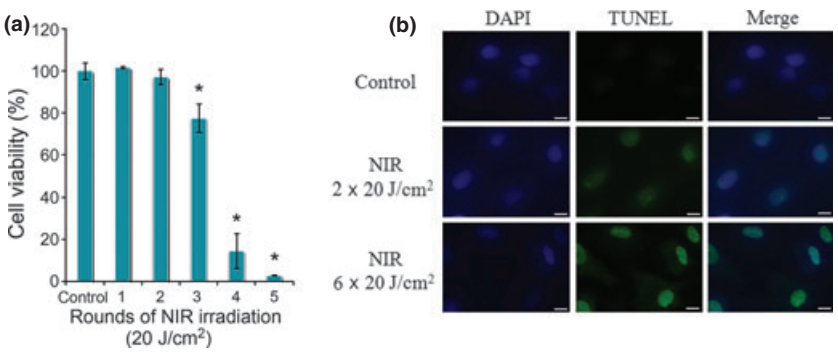

Fig. 1. (a) Cytotoxicity of near-infrared (NIR) irradiation treatment of A549 cells evaluated using the MTT assay. (b) Apoptotic cell death in A549 cells. After 3h NIR irradiation treatment, A549 cells were stained by the TUNEL method to detect apoptotic cells and nuclei were subsequently counterstained by DAPI. Scale lines, 10 μm.

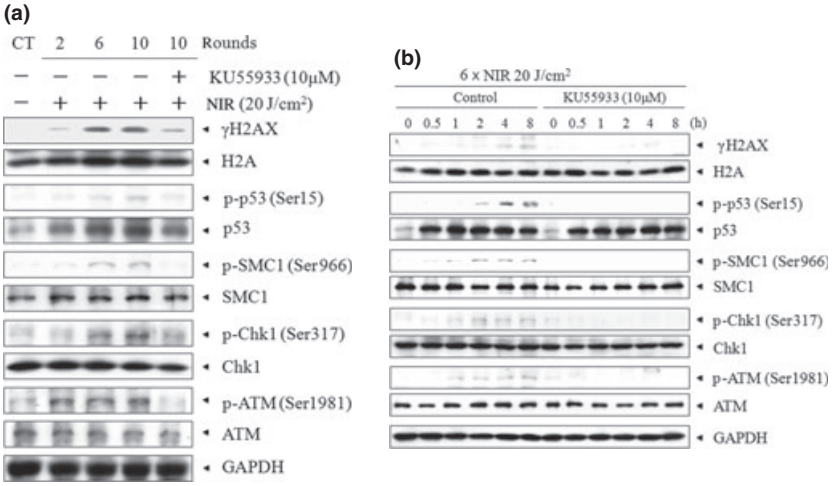

Fig. 2. Immunoblot analysis of A549 cells treated with near-infrared (NIR) irradiation. (a) To clarify whether NIR irradiation induces a DNA damage response that includes the checkpoint signaling pathway, the phosphorylation of DNA damage checkpoint proteins, such as histone H2AX, p53, structural maintenance of chromosome (SMC) 1 , Chk1, and ataxia-telangiectasia mutated (ATM), was evaluated after two to six rounds of NIR irradiation at 20 J/cm^2. (b) Time-dependent phosphorylation of DNA damage checkpoint molecules after six rounds of treatment with 20 J/cm^2 NIR irradiation was observed, in the absence or presence of the ATM-specific inhibitor KU55933, between 0 and 8 h. p-, phosphorylated.

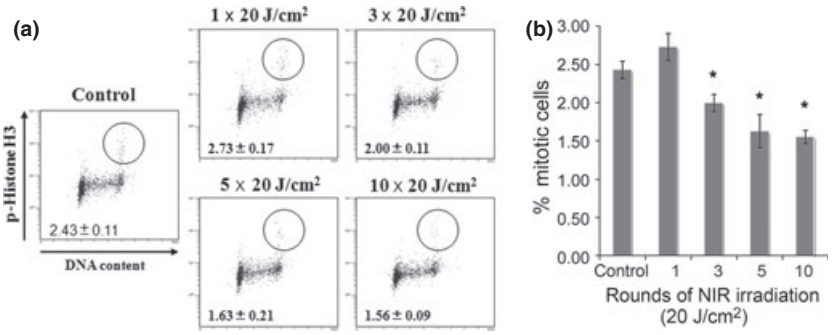

Fig. 3. (a) Analysis of the G_2/M checkpoint. The mitotic transition was examined by flow cytometric analysis to assess the effect of the cellular DNA damage response induced by different rounds of near-infrared (NIR) irradiation at 20 J/cm^2. (b) Data obtained in (a) were analyzed using XL2 software (Beckman Coulter, Brea, CA, USA) to determine the percentage of mitotic cells. Data are the mean ± SD ($n > 3$). *$P < 0.05$ compared with control.

Furthermore, the application of NIR irradiation did not cause pain to the mice, because they did not withdraw even though NIR irradiation was performed without anesthesia.

Immunoblot analysis of tumor samples. We further examined whether the treatment of NIR can activate the DNA damage response in tumors. We found that NIR increased the phosphorylation of H2AX, p53 at Ser^{15}, SMC1 at Ser^{966}, and Chk1 at Ser^{317} in tumor tissues (Fig. 6). Similarly, DOX increased the phosphorylation of p53, SMC1, and Chk1 at these sites (Fig. 6). These data indicate that each checkpoint protein is activated by NIR treatment through ATM activation.

Discussion

The present study has demonstrated that a specific wavelength of NIR irradiation, which simulates solar NIR with pre- and parallel-irradiational cooling, can non-thermally induce cytocidal effects in cancer cells by inducing DNA damage. Near-infrared is an electromagnetic wave that simultaneously exhibits both wave and particle properties and is absorbed by sweat on the skin surface, water in the dermis,[2] hemoglobin in dilated vessels,[2,9] myoglobin in superficial muscles,[5,6] and bone cortical mass.[8] Near-infrared can non-thermally induce the degeneration of myoglobin, which results in apoptosis of vascular smooth muscle cells and marked long-lasting vasodilation. Near-infrared penetrates superficial layers and is absorbed by chromophores, such as hemoglobin and myoglobin,[21,22] which are oxygen-carrying proteins that have many α-helices.[10,23,24] The α-helices have strong amide bands in the infrared spectra that have characteristic frequencies and intensities[25] and are thought to be involved in the resonance by NIR.[10] Therefore, NIR may induce the resonance of α-helices in these oxygen-carrying proteins, resulting in protein degeneration, damage to oxygen storage and transport, and apoptosis.[10]

Previously, NIR was been reported to induce cell death by apoptosis.[14] Actively proliferating cells also show increased sensitivity to red and NIR radiation.[12,13]

The NIR spectrum of biological materials is a result of the overtones and combination of O-H, C-H, and N-H group bond stretching vibrations.[26] It is hypothesized that NIR mainly resonates helical structures, α-helices, and DNA.[10] Moreover, it is predicted that NIR induces DNA damage, and this could be one of the mechanisms underlying apoptosis. However, to date there is no evidence demonstrating the effects of NIR on cellular DNA damage checkpoint signals.

In the present study, we used an NIR device emitting a spectrum of NIR irradiation from 1100 to 1800 nm with a water filter that excluded wavelengths between 1400 and 1500 nm, which are strongly absorbed by water and hemoglobin. By

doi: 10.1111/j.1349-7006.2012.02310.x

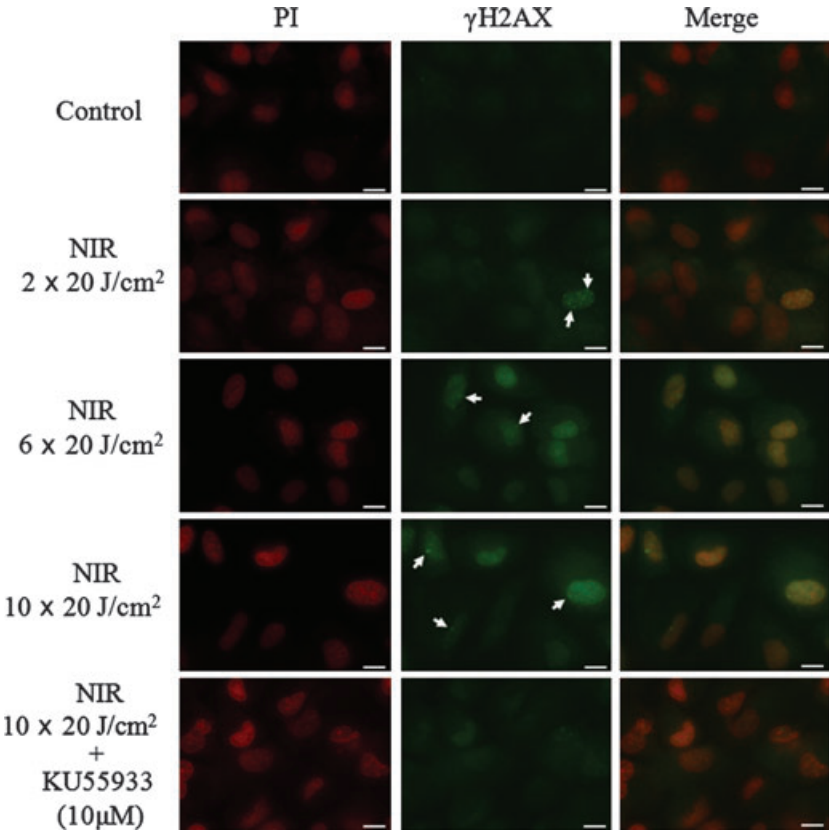

Fig. 4. Formation of γH2AX foci in A549 cells after 3 h of near-infrared (NIR) irradiation, in the absence or presence of the ataxia-telangiectasia mutated (ATM)-specific inhibitor KU55933. The arrows indicate γH2AX foci in nuclei. Cell nuclei were counterstained with propidium iodide (PI). Scale lines, 10 μm.

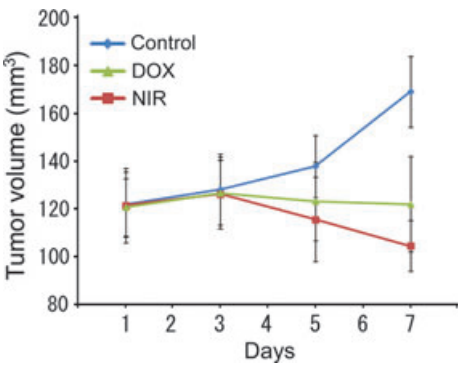

Fig. 5. Relative tumor volume of the MDA-MB435 xenograft. Near-infrared (NIR) irradiation induced marked cytocidal tumor shrinkage compared with control after seven rounds of NIR treatment at 40 J/cm^2, whereas doxorubicin (DOX) only statically inhibited the tumor growth of MDA-MB435 tumors in nude mice.

filtering out wavelengths below 1100 nm, around 1450 nm, and above 1850 nm, NIR irradiation can reach deeper tissues.[27] However, an NIR device increases skin surface temperature and induces perspiration and blood vessel dilation, even with a water filter, which mediates the absorption of NIR radiation by water and hemoglobin. To counter this effect, in the present study we used contact cooling through a temperature-controlled sapphire window to reduce the skin surface temperature and thereby reduce perspiration and blood vessel dilation. These specific wavelengths and the cooling system

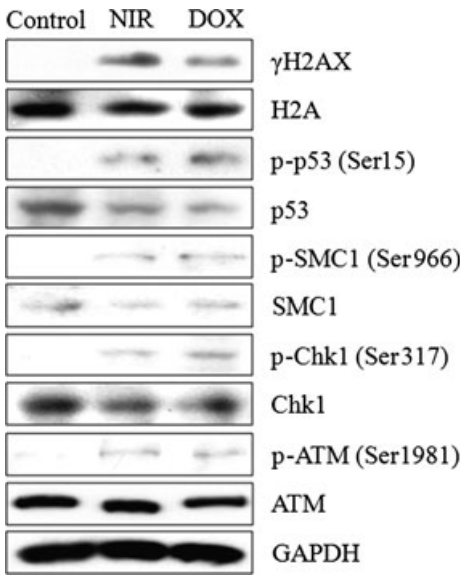

Fig. 6. Immunoblot analysis of xenograft tumor samples. We examined whether treatment with near-infrared (NIR) irradiation also activated the DNA damage response in tumors. We showed that doxorubicin (DOX) increased the phosphorylation of p53 at Ser^{15}, structural maintenance of chromosome (SMC) 1 at Ser^{966}, and Chk1 at Ser^{317} in tumor samples. Similarly, NIR irradiation increased the phosphorylation of p53, SMC1, and Chk1. p-, phosphorylated; ATM, ataxia-telangiectasia mutated.

enabled NIR irradiation to penetrate the skin surface without pain or epidermal burns,[27,28] which was evident by the ability to treat mice without anesthesia. Moreover, contact burns or other adverse events were not observed.

In our previous study, we demonstrated that A549 lung adenocarcinoma cells responded well to DNA damage induced by ultraviolet and γ-irradiation.[29] In addition, several DNA damage checkpoint signals have been discovered using A549 cells.[30,31] Therefore, the A549 cell line provides a good *in vitro* model for understanding how NIR modulates cellular signal transduction related to the DNA damage response pathway. In the present study, A549 cell proliferation was significantly inhibited by NIR irradiation and this was due to apoptosis, as expected. Total NIR output appeared to correlate with cell survival. In addition, the correlation with efficacy seemed to be highest with the total amount of energy delivered and not the per pulse fluence, because multiple rounds of irradiation with a lower output appeared equally effective as higher fluence irradiation. Ten exposures at 20 J/cm^2 achieved a comparable significant reduction in cell count as that of three exposures at 40 J/cm^2.[7] In addition, three exposures at 20 J/cm^2 appeared to be close to an *in vitro* threshold energy dosage in the present study, as well as in our previous studies.[7,10]

To determine whether NIR induces a DNA damage response, including the checkpoint signaling pathway, the phosphorylation of H2AX at Ser^{139} was measured as an index of the DNA damage of cells.[32] After treatment with NIR, phosphorylation of H2AX occurred after two rounds of NIR at 20 J/cm^2. The formation of γH2AX foci was clearly observed in NIR irradiation-treated cells. Ataxia-telangiectasia mutated is a key molecule in the DNA damage response[33] and was clearly phosphorylated at Ser^{1981} after NIR irradiation. We also confirmed the dose-dependent phosphorylation of several DNA damage checkpoint molecules, including Ser^{15} of p53, Ser^{966} of SMC1, and Ser^{317} of Chk1 by NIR irradiation. Notably, KU55933, an ATM-specific inhibitor,[34] markedly decreased the phosphorylation of checkpoint molecules. These results indicate that ATM is activated by NIR irradiation and transduces the downstream activation of other factors in the pathway. Therefore, our findings indicate that NIR irradiation exerts checkpoint signals by damaging cellular DNA.

We further examined the mitotic transition of cells using flow cytometry to assess the effect of the cellular DNA damage response by NIR. The percentage of mitotic A549 cells was evaluated by histone H3 phosphorylation at Ser^{10},[35] and was found to be significantly decreased after more than three rounds of NIR irradiation at 20 J/cm^2. These data indicate that the G_2/M checkpoint is activated by NIR-induced DNA damage to avoid mitotic error.

Near-infrared irradiation suppresses the proliferation of various kinds of malignant cells and damages highly proliferative cells, such as bone marrow cells.[8] In our *in vivo* studies, we used MDA-MB435 cells because they develop highly proliferative skin neoplasms that appear to be susceptible to solar and artificial NIR irradiation. Near-infrared irradiation induced marked cytocidal tumor shrinkage compared with control after seven rounds of NIR treatment at 40 J/cm^2, whereas DOX only statically inhibited MDA-MB435 tumor growth in nude mice. We further examined whether NIR irradiation treatment also activates the DNA damage response in tumors and found that NIR irradiation increased the phosphorylation of p53 at Ser^{15}, SMC1 at Ser^{966}, and Chk1 at Ser^{317} in the tumor samples. Similarly, DOX increased the phosphorylation of p53, SMC1, and Chk1 at these sites as well. These data indicate that each checkpoint protein was activated by NIR irradiation treatment via ATM activation.

The ATM protein kinases act as master controllers in DNA damage checkpoint signaling.[36] In a previous study, ATM-deficient cells, derived from human ataxia telangiectasia (AT) patients, were found to exhibit chromosomal instability, telomere shortening, and defects in cellular responses to DNA double-strand breaks following exposure to infra-red and radiomimetic chemicals, including DOX.[37] The results of the present study indicate that NIR irradiation causes cytocidal effects in cancer cells by inducing double-strand DNA breaks in an *in vivo* tumor model.

In our previous *in vivo* studies, histological findings showed tumor shrinkage and cell death in the center of the tumor mass, which supports the hypothesis that NIR electromagnetic properties non-thermally induce the biological effects observed.[7,10] Near-infrared irradiation penetrates the skin and reaches the subcutaneous tissues without a significant increase in skin temperature,[38] and the effects of NIR irradiation are independent of the generation of heat.[39] If the cytocidal effect of NIR irradiation was induced thermally, the histology would have shown a gradient cytocidal effect from the superficial layer to the center of the tumor, and the thermal effect would be reduced by the contact cooling (20°C) of the NIR device. Due to surface cooling, NIR irradiation can penetrate deeper tissue and induce a marked non-thermal cytocidal effect in the center of the tumor mass. Furthermore, NIR irradiation treatment with very low output and fewer exposures (10 exposures of NIR at 20 and 40 J/cm^2) also inhibited tumor growth. This output was so low that, on human skin, the sensation of heat would not be felt because of contact cooling. The NIR irradiation induced no pain and the mice did not withdraw from the treatment even though NIR treatment was performed without anesthesia. In addition, side effects, such as epidermal burns, were not observed and the mice appeared to be healthy throughout the study. Further studies are necessary to determine whether more output, increased frequency of treatments, or longer periods of irradiation may be even more effective in suppressing tumor growth.

There are several advantages of the NIR irradiation schedule determined in the present study, including a reduction in discomfort, limited side effects, and low cost. These characteristics were facilitated by repeated rounds of irradiation, which, if proven beneficial for cancer cell reduction in humans, may provide an alternative or adjunct treatment for transient mass reduction before surgery and could provide improved results and quality of life for patients. Near-infrared irradiation is frequently administered at a level of 40 J/cm^2 for other indications and has a very high safety record with no significant complications.[28] It should be noted that the present study was a preliminary study based on experiments in a limited variety of cancer cell lines. Additional studies are warranted in larger numbers and various types of cancer cell types and with longer post-treatment periods to evaluate the variations in treatment parameters and correlations with other antitumor therapies. Importantly, however, these studies hold promise in the design of more efficacious cancer treatments.

Acknowledgments

The authors thank Dr Masaji Ishiguro (Niigata University of Pharmacy and Applied Life Sciences [NUPALS], Niigata, Japan) for the critical reading of this manuscript, Mr Yasuhiro Nakajima (NUPALS) for his support with the NIR irradiation treatment, and Miss Chika Washio (NUPALS) for her support with the cell culture and flow cytometry.

Disclosure Statement

None of the authors of has any conflict of interest to disclose.

doi: 10.1111/j.1349-7006.2012.02310.x

References

1 Tanaka Y, Matsuo K, Yuzuriha S, Shinohara H. Differential long-term stimulation of type I versus type III collagen after infrared irradiation. *Dermatol Surg* 2009; **35**: 1099–104.
2 Tanaka Y, Matsuo K, Yuzuriha S. Long-term evaluation of collagen and elastin following infrared (1100 to 1800 nm) irradiation. *J Drugs Dermatol* 2009; **8**: 708–12.
3 Tanaka Y, Matsuo K, Yuzuriha S. Long-term histological comparison between near-infrared irradiated skin and scar tissues. *Clin Cosmet Investig Dermatol* 2010; **3**: 143–9.
4 Tanaka Y, Matsuo K, Yuzuriha S. Objective assessment of skin rejuvenation using near-infrared 1064-nm neodymium:YAG laser in Asians. *Clin Cosmet Investig Dermatol* 2011; **4**: 123–30.
5 Tanaka Y, Matsuo K, Yuzuriha S. Long-lasting muscle thinning induced by infrared irradiation specialized with wavelength and contact cooling: a preliminary report. *ePlasty* 2010; **10**: e40.
6 Tanaka Y, Matsuo K, Yuzuriha S. Long-lasting relaxation of corrugator supercilii muscle contraction induced by near infrared irradiation. *ePlasty* 2011; **11**: e6.
7 Tanaka Y, Matsuo K, Yuzuriha S, Yan H, Nakayama J. Non-thermal cytocidal effect of infrared irradiation on cultured cancer cells using specialized device. *Cancer Sci* 2010; **101**: 1396–402.
8 Tanaka Y, Matsuo K, Yuzuriha S. Near-infrared irradiation non-thermally affects subcutaneous adipocytes and bones. *ePlasty* 2011; **11**: e12.
9 Tanaka Y, Matsuo K, Yuzuriha S. Near-infrared irradiation non-thermally induces long-lasting vasodilation by causing apoptosis of vascular smooth muscle cells. *ePlasty* 2011; **11**: e22.
10 Tanaka Y, Matsuo K. Non-thermal effects of near-infrared irradiation on melanoma. In: Tanaka Y ed. *Breakthroughs in Melanoma Research*. Croatia: InTech, 2011. Available from: http://www.intechopen.com/books/breakthroughs-in-melanoma-research (accessed 2 Apr 2012).
11 Santana-Blank LA, Rodriguez-Santana E, Vargas F *et al.* Phase I trial of an infrared pulsed laser device in patients with advanced neoplasias. *Clin Cancer Res* 2002; **8**: 3082–91.
12 Karu T, Pyatibrat L, Kalendo G. Irradiation with He-Ne laser can influence the cytotoxic response of HeLa cells to ionizing radiation. *Int J Radiat Biol* 1994; **65**: 691–7.
13 Tafur J, Mills PJ. Low-intensity light therapy: exploring the role of redox mechanisms. *Photomed Laser Surg* 2008; **26**: 321–6.
14 Tirlapur UK, König K. Femtosecond near-infrared laser pulse induced strand breaks in mammalian cells. *Cell Mol Biol* 2001; **47**: 131–4.
15 Dees C, Harkins J, Petersen MG, Fisher WG, Wachter EA. Treatment of murine cutaneous melanoma with near infrared light. *Photochem Photobiol* 2002; **75**: 296–301.
16 Shiloh Y. ATM and ATR: networking cellular responses to DNA damage. *Curr Opin Genet Dev* 2001; **11**: 71–7.
17 Abraham RT. Cell cycle checkpoint signaling through the ATM and ATR kinases. *Genes Dev* 2001; **15**: 2177–96.
18 Wright JA, Keegan KS, Herendeen DR *et al.* Protein kinase mutants of human ATR increase sensitivity to UV and ionizing radiation and abrogate cell cycle checkpoint control. *Proc Natl Acad Sci USA* 1998; **95**: 7445–50.
19 Shigeta T, Takagi M, Delia D *et al.* Defective control of apoptosis and mitotic spindle checkpoint in heterozygous carriers of ATM mutations. *Cancer Res* 1999; **59**: 2602–7.
20 Shackelford RE, Innes CL, Sieber SO, Heinloth AN, Leadon SA, Paules RS. The ataxia telangiectasia gene product is required for oxidative stress-induced G_1 and G_2 checkpoint function in human fibroblasts. *J Biol Chem* 2001; **276**: 2.
21 Ferrari M, Mottola L, Quaresima V. Principles, techniques, and limitation of near infrared spectroscopy. *Can J Appl Physiol* 2004; **29**: 463–87.
22 Nancini DM, Bolinger L, Li H, Kendrick K, Chance B, Wilson JR. Validation of near-infrared spectroscopy in humans. *J Appl Physiol* 1994; **77**: 2740–7.
23 Kendrew JC, Dickerson RE, Strandberg BE *et al.* Structure of myoglobin: a three-dimensional Fourier synthesis at 2 A resolution. *Nature* 1960; **185**: 422–7.
24 Schlichting I, Chu K. Trapping intermediates in the crystal: ligand binding to myoglobin. *Curr Opin Struct Biol* 2000; **10**: 744–52.
25 Nevskaya NA, Chirgadze YN. Infrared spectra and resonance interactions of amide-I and II vibrations of alpha-helix. *Biopolymers* 1976; **15**: 637–48.
26 Weyer LG. Near-infrared spectroscopy of organic substances. *Appl Spectrosc Rev* 1985; **21**: 1–43.
27 Davenport SA, Gollnick DA, Levernier M, Spooner GJR. *Method and System for Treatment of Post-Partum Abdominal Skin Redundancy or Laxity*. (US) patent no. 20060052847. 2005; 8 Aug.
28 Goldberg DJ, Hussain M, Fazeli A, Berlin AL. Treatment of skin laxity of the lower face and neck in older individuals with a broadspectrum infrared light device. *J Cosmetic Laser Ther* 2007; **9**: 35–40.
29 Nishida H, Tatewaki N, Nakajima Y *et al.* Inhibition of ATR protein kinase activity by schisandrin B in DNA damage response. *Nucleic Acids Res* 2009; **37**: 5678–89.
30 Sarkaria JN, Busby EC, Tibbetts RS *et al.* Inhibition of ATM and ATR kinase activities by the radiosensitizing agent, caffeine. *Cancer Res* 1999; **59**: 4375–82.
31 Winsel S, Sommer A, Eschenbrenner J *et al.* Molecular mode of action and role of TP53 in the sensitivity to the novel epothilone sagopilone (ZK-EPO) in A549 non-small cell lung cancer cells. *PLoS ONE* 2011; **6**: e19273.
32 Paull TT, Rogakou EP, Yamazaki V, Kirchgessner CU, Gellert M, Bonner WM. A critical role for histone H2AX in recruitment of repair factors to nuclear foci after DNA damage. *Curr Biol* 2000; **10**: 886–95.
33 Bakkenist CJ, Kastan MB. DNA damage activates ATM through intermolecular autophosphorylation and dimer dissociation. *Nature* 2003; **421**: 499–506.
34 Hickson I, Zhao Y, Richardson CJ *et al.* Identification and characterization of a novel and specific inhibitor of the ataxia-telangiectasia mutated kinase ATM. *Cancer Res* 2004; **64**: 9152–9.
35 Zeitlin SG, Barber CM, Allis CD, Sullivan KF. Differential regulation of CENP-A and histone H3 phosphorylation in G_2/M. *J Cell Sci* 2001; **114**: 653–61.
36 Shiloh Y. ATM and related protein kinases: safeguarding genome integrity. *Nat Rev Cancer* 2003; **3**: 155–68.
37 Kurz EU, Douglas P, Lees-Miller SP. Doxorubicin activates ATM-dependent phosphorylation of multiple downstream targets in part through the generation of reactive oxygen species. *J Biol Chem* 2004; **279**: 53272–81.
38 Schieke SM, Schroeder P, Krutmann J. Review article. Cutaneous effects of infrared radiation: from clinical observations to molecular response mechanisms. *Photodermatol Photoimmunol Photomed* 2003; **19**: 228–34.
39 Danno K, Mori N, Toda K, Kobayashi T, Utami A. Near-infrared irradiation stimulates cutaneous wound repair: laboratory experiments on possible mechanisms. *Photodermatol Photoimmunol Photomed* 2001; **17**: 261–5.